Tina Memo No. 2007-006
Published in AJNR, 2007, vol, 28 pp. 983-989.

Prediction of the Jugular Venous Waveform using a Model of Cerebrospinal Fluid Dynamics

J. Kim, P.A. Bromiley, N.A. Thacker and A. Jackson

Last updated
23 / 3 / 2008

Imaging Science and Biomedical Engineering Division,
Medical School, University of Manchester,
Stopford Building, Oxford Road,
Manchester, M13 9PT.

Prediction of the Jugular Venous Waveform using a Model of Cerebrospinal Fluid Dynamics

J. Kim, P.A. Bromiley, N.A. Thacker and A. Jackson
Dept. of Medical Biophysics
Imaging Science and Biomedical Engineering Division
Medical School, University of Manchester
Manchester, M13 9PT, UK
neil.thacker@man.ac.uk

Abstract

Background and Purpose: We have previously reported a model of cerebral hydrodynamics in the form of an equivalent electrical circuit. The aim of this work was to demonstrate that the model could predict venous flow patterns seen in the superior sagittal sinus, straight sinus and jugular vein in normal volunteers.
Methods: An electrical equivalence model of cerebro-spinal fluid (CSF) and cerebral blood flow was fitted to measured arterial and CSF data from 16 normal volunteers. Predictions of the venous outflow waveform derived from the model were compared to measured venous flows in the superior sagittal sinus (SSS), straight sinus (STS) and jugular vein (JV).
Results: The model accurately predicted the measured jugular waveform. The measured waveforms from SSS and STS showed a less pronounced and delayed systolic peak compared to the predicted outflow. The fitted bulk model parameters provided relative values that correspond approximately to the impedance of arterial capillaries (1.0), cerebral aqueduct (≈ 0), venous capillaries (≈ 0), and arteries (0.01) and for the elastic capacitance of the ventricles (4.11), capillaries (≈ 0), and veins (271). The elastic capacitance of the major cerebral arteries was large and could not be accurately determined.
Conclusions: We have confirmed the ability of the model to predict the venous waveforms in normal individuals. The absence of any statistically significant component of the venous waveform not described by the model implies that measurements of venous flow could be used to constrain further the model fitting process.

1 Introduction

The Monro-Kellie hypothesis states that the sum of the brain, CSF and intracranial blood volumes is constant if the skull is intact [10]. ECG (electrocardiogram) gated magnetic resonance (MR) phase imaging allows quantitative, high temporal resolution imaging of CSF and blood flow within the skull during a single cardiac cycle. MR-based studies of these flows show that the constraints of the Monro-Kellie hypothesis result in a complex homeostatic hydrodynamic mechanism, which compensates for the transient increases in cerebral blood volume and arterial blood pressure occurring during systole [3, 11]. We refer to this as Monro-Kellie homeostasis to distinguish it from the mechanisms responsible for the maintenance of mean cerebral blood flow. Breakdown of Monro-Kellie homeostasis has been implicated in a number of disease processes [3, 11, 4, 5, 6, 7, 9, 12, 13].

Almost all previous magnetic resonance imaging (MRI) studies rely on phenomenological observations such as flow volume measurements or delay in the arteriovenous passage of the systolic pulse wave, or first-order derived variables describing more physiological parameters, notably vascular compliance within the vascular tree feeding specific venous drainage territories [3]. Unfortunately, the complexity of the homeostatic mechanism, common variations in vascular anatomy [3, 2, 8], variation in measurements and interpretation methods recommended by different groups [11, 5, 6, 18, 14, 21] and the limitations on the number of measurements available from MRI flow techniques combine to make these approaches increasingly unsatisfactory. There is a clear need for a quantitative physiological model to act as a substrate for principled analysis of this type of data to support direct comparison between studies and, more importantly, allow estimation of hydrodynamic parameters that cannot be measured directly with existing techniques.

We have recently reported a model, which describes the interrelationships between arterial, capillary and venous blood flow and movements of CSF between the cerebral ventricles, subarachnoid and spinal CSF spaces [15, 16], using an electrical circuit analogy. When fitted to arterial and foramen magnum flow measurements it allows direct

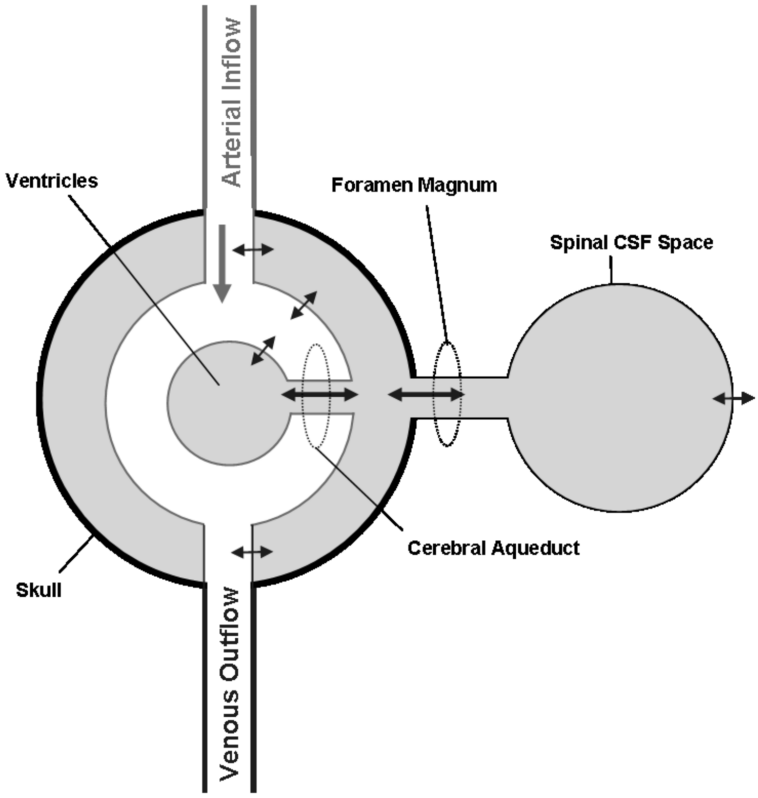

Figure 1: The simplified anatomical model on which the electrical equivalence model is based. Boundaries identified by thin lines are considered compliant.

proportional (but not absolute) estimation of seven parameters that cannot be derived by direct measurement, corresponding approximately to arterial, brain, ventricular and venous compliances, and arterial, brain and cerebral aqueduct impedances. The identification of additional localised, measurable inputs that can be used to drive the fitting process could provide more anatomical specificity. Fortunately the existing model provides the ideal method to investigate the validity of such additional measurements since observed values can be directly compared with model-based predictions. The objective of this study is therefore to demonstrate that the model can predict venous flow patterns seen in the superior sagittal sinus, straight sinus and jugular vein in normal volunteers.

2 Methods

2.1 Electrical Equivalence Model

The electrical equivalence model has been presented previously [15, 16]. In brief, it is based on the simplified anatomical construct illustrated in Figure 1. This idealised system is modelled, treating the impedance of flow paths as resistances, the compliance of thin boundaries as capacitances, pressure differences as voltages and flows as currents. This results in the electrical equivalence model shown in Figure 2a. Analysis of this model illustrates redundancy of some components, supporting simplification to the final circuit demonstrated in Figure 2b. A series of functions that can be fitted using standard minimisation approaches can then be derived (See Appendix 1).

2.2 Subjects and MR Image Acquisition

MR image volumes were acquired from 16 control subjects (14 male and 2 female, age 32 ± 10 yrs) with no known abnormality. Written informed consent was obtained from all subjects and the local NHS (National Health Service) and University ethical committees approved the study. All subjects were scanned using a 3T whole body imager (Acheiva, Philips Medical Systems, Best, NL). Sagittal T1-weighted images and phase-contrast (PC) angiography scout images were acquired to allow prescription of imaging planes perpendicular to the principal direction of flow (Figure 3). Velocity encoded PC-cine MR images were then obtained at 7 points: CSF flow at the cerebral

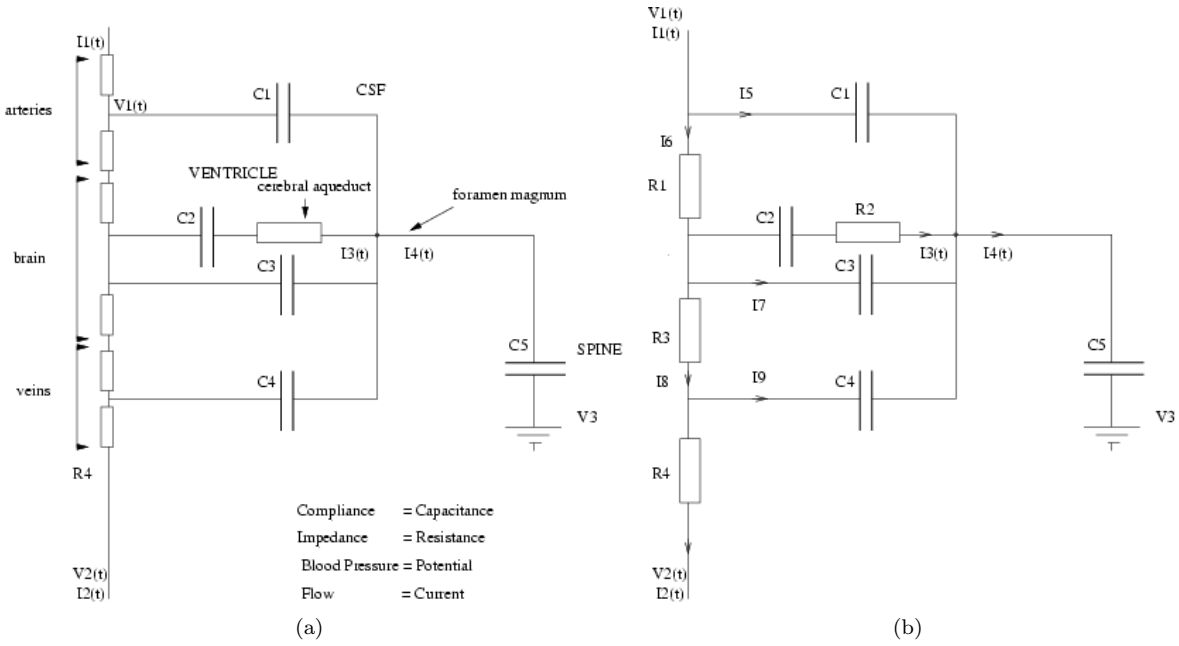

Figure 2: (a) The electrical equivalence model derived from the anatomical model shown in Fig.1. (b) The simplified equivalent circuit after removal of redundant components.

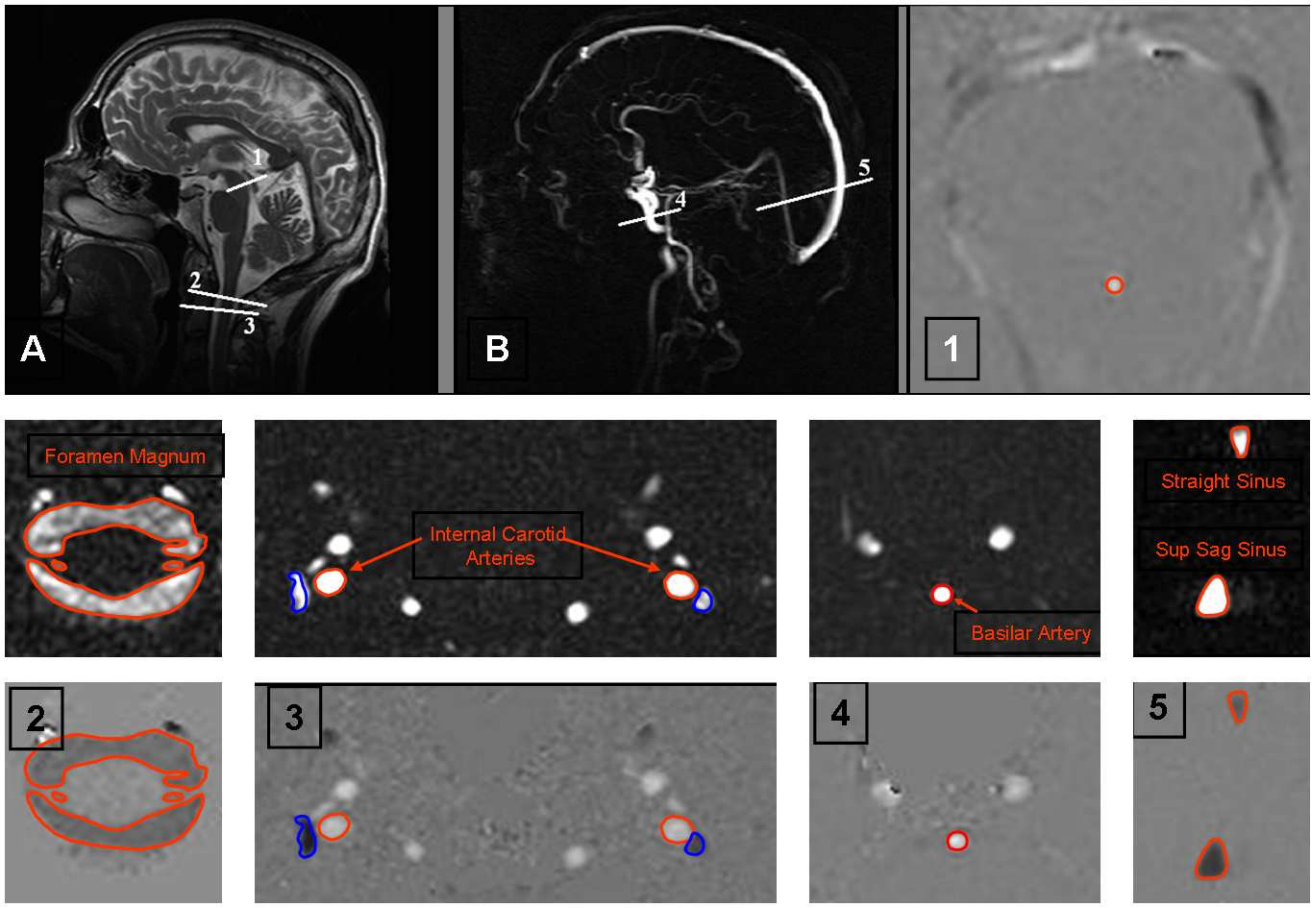

Figure 3: Anatomical (A) and artiographic (B) scout images showing the location of the measurement planes. Subsequent images show the location of regions of interest for the cerebral aqueduct (1), foramen magnum (2), internal carotid arteries and jugular veins (3), basilar artery (4) and superior sagittal and straight sinuses (5).

	Volume	PI (mean±stdev)
SSS	305.79 ± 53.59	0.33 ± 0.057
STS	87.23 ± 16.61	0.28 ± 0.068
Ven	392 ± 61.4	0.31 ± 0.041
JV	312 ± 138	0.51 ± 0.045
CAB	536.21 ± 73.61	0.81 ± 0.21
I2	536.21 ± 71.14	0.45 ± 0.16
I8	$--$	0.0037 ± 0.0013
I9	$--$	1.91 ± 0.53

Table 1: The measured flow volumes (mls/minute) and pulsatility indices from the superior sagittal sinus (SSS), straight sinus (STS), combined venous outflow (SSS+STS=Ven), jugular vein and arterial inflow (carotid+basilar arteries=CAB), the predicted flow volume for I2 (overall venous outflow in the model), and the predicted indices for I2, I8 and I9.

aqueduct (AQ); CSF flow at the foramen magnum (FM); arterial blood flow in the basilar artery (BA) at the level of the mid-clivus; arterial blood flow in the internal carotid arteries (CA) immediately below the foramen lacerum; venous blood flow from the superior sagittal sinus (SSS) 2-3 cm above the confluence of the sinuses; venous blood flow from the midpoint of the straight sinus (STS); venous blood flow from the jugular veins immediately below the base of skull (JV). Two of the JV images exhibited motion artefacts, which prevented accurate location of the vessel, and so only 14 JV images were used in the subsequent analysis. Retrospective vector electrocardiographic gating was used to generate 16 pairs of images spanning the cardiac cycle for each subject. The first image was a flow modulus image showing the anatomical location of flow and the second a velocity-encoded image in which the intensity is linearly proportional to flow velocity (Figure 3). The imaging parameters were: flip angle $10 - 15^o$; slice thickness 5-7mm; repetition time 8.82-22.13ms; and echo time 8.14-14.39ms; velocity encoding (Venc) was set at 10cm/sec for the AQ and FM, 90cm/sec for the BA and CA, and 60cm/sec for SSS, STS and JV. Scan time was usually 2-4 min for each region depending on heart rate; total scanning time was 15-30min.

2.3 Image processing

In order to obtain a reliable estimation of the AQ flow, an approximate location for the centre of the aqueduct was provided manually and a quadratic function was fitted over the nine voxels in a 3x3 region around it at each time point in the cardiac cycle. The area under this curve was then integrated for all positive values of the function. The BA, CA, FM, SSS, STS and JV flows were estimated from the sum of flow values within the region of the vessels, defined by thresholding the modulus images to find the region of interest (ROI) as shown in Figure 3.

2.4 Data Analysis

Measured values from CA and BA were combined to produce an arterial input function (CAB). The flow values from CAB, FM and AQ were then used to fit the model allowing prediction of venous outflow currents corresponding to I8, I9 and I2 in Figure 2B. Measured flow values from SSS and STS were summed to derive an estimated total supratentorial venous output function (Ven). Measured values of flow in SSS, STS, Ven and JV were compared with predicted values for venous outflow from the model (I2). Waveforms were compared using Wald-Wolfowitz runs test for mean values and Mann Whitney test for comparison of group data at each individual heart phase. Pulsatility indices were calculated for SSS, ST, JV, I8, I9 and I2 by subtracting the end diastolic flow rate from the peak systolic flow rate and dividing by the average value [4]. Pulsatility indices were compared using the Mann Whitney test.

3 Results

Table 1 shows the range of measured values of flow in the CAB, SSS, STS and JV and model based predictions of I2, I8 and I9 for all 16 subjects. The measured SSS flow showed considerable variation from 34-75% of the combined carotid and basilar artery (CAB) flows reflecting the anatomical variation in prosencephalic venous drainage described by previous authors [8]. The total STS flow also showed significant but smaller variation from 11-21% of CAB whilst the combined SSS and STS measurements accounted for between 46-92% of measured CAB. The combined JV measurements were also extremely variable accounting for 48-104% of the measured CAB in

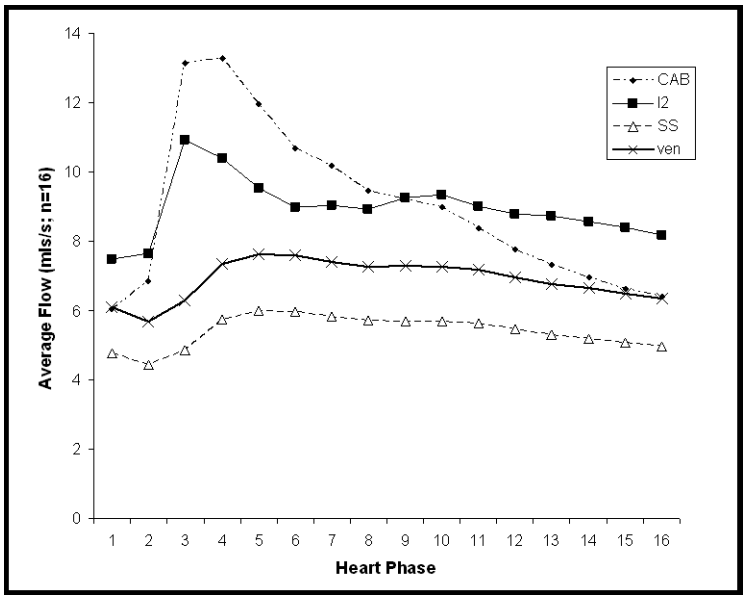

Figure 4: Measured flow rates for carotid and basilar arteries combined (CAB), superior saggital sinus (SSS) and combined straight sinus (STS) and SSS venous outflow (Ven) averaged across 16 subjects compared to the predicted venous outflow I2.

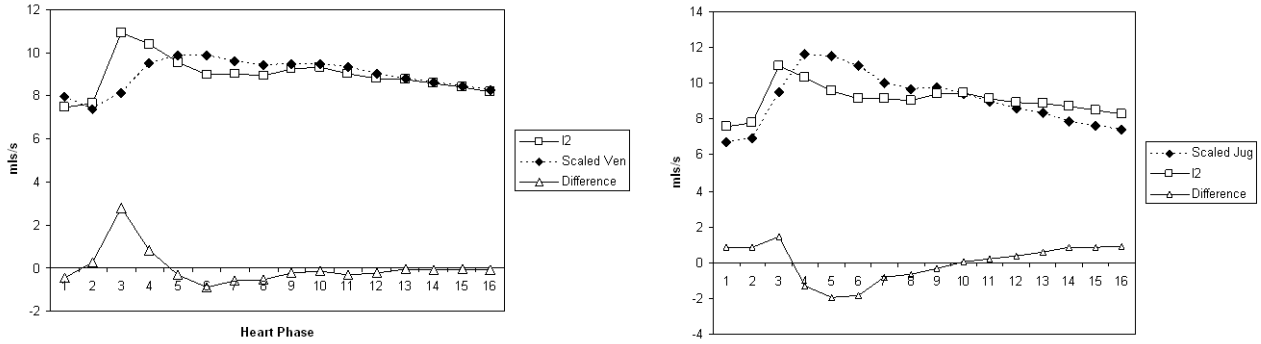

(a) (b)

Figure 5: (a) Comparison of the predicted venous outflow (I2) and the combined STS and SSS venous outflow (Ven). The venous outflow has been scaled to have the same integral as I2. The lower curve shows the difference in the waveforms. Note the prominent systolic peak in the difference. (b) Comparison of the predicted venous outflow (I2) and the jugular venous outflow (JV). The venous outflow has been scaled to have the same integral as I2. The lower curve shows the difference in the waveforms.

keeping with the observations of previous authors [8]. The presence of Ven flows equivalent to CAB presumably reflects the use of a BA measurement point distal to the inferior cerebellar and other inferior arterial branches within the infra-tentorial compartment. Similarly the observation of JV flows in excess of the CAB presumably reflects the combination of this factor and contributions of the extra-cerebral circulation to jugular venous drainage.

Comparison of the pulsatility indices of the observed and measured parameters (Table 1) showed that the measured values of SSS, STS and Ven were significantly lower (0.33 ± 0.057, $p < 0.05$; 0.28 ± 0.068, $p < 0.01$; 0.31 ± 0.041, $p < 0.05$) than the predicted value for I2 (0.45 ± 0.16). The pulsatility index of JV (0.51 ± 0.045) was not significantly different from I2.

Figure 4 shows the time course curves from a single cardiac cycle for mean values of CAB, I2, SSS and Ven. These represent the interactions occurring within the supratentorial compartment. It can be seen that SSS and Ven have identical curve shapes and represent approximately 70% of the predicted value of I2. In addition there is a significant delay of approximately 12% of a cardiac cycle between the systolic peak of the CAB and I2 curves and the measured data from SSS and Ven.

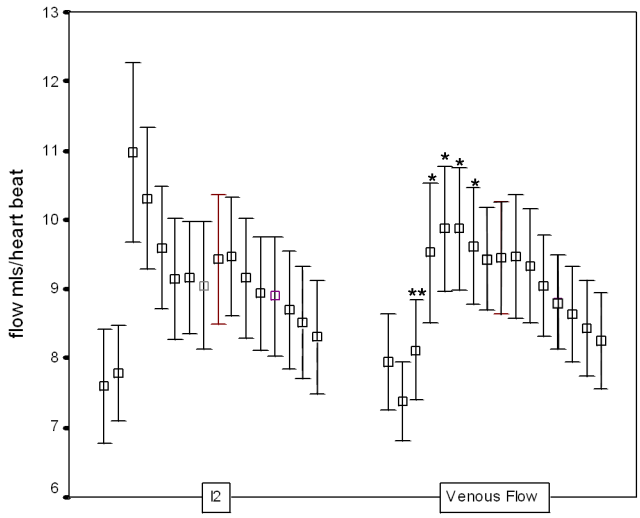

Figure 6: Mean and 95% confidence intervals for flow at each of 16 heart phases for the predicted venous outflow (I2) and the combined STS and SSS venous outflow (Ven). Asterisks indicate significant differences ($* = p < 0.05$, $** = p < 0.01$).

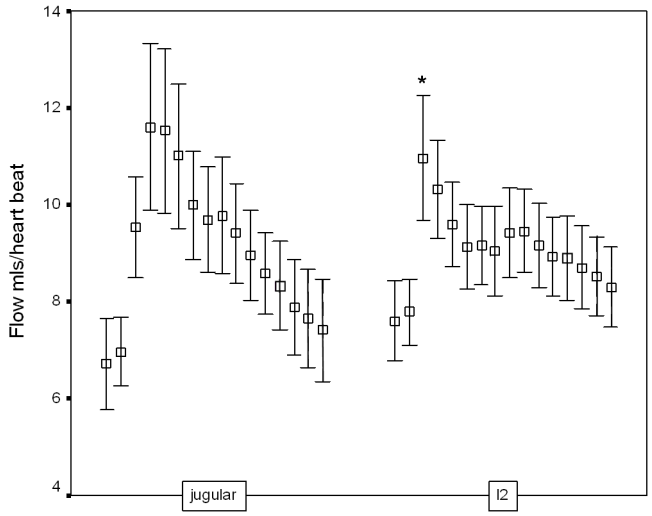

Figure 7: Mean and 95% confidence intervals for flow at each of 16 heart phases for the predicted venous outflow (I2) and the jugular venous outflow. Asterisks indicate significant differences ($* = p < 0.05$).

Figure 5a shows the time course of I2 and Ven (scaled to I2 i.e. equivalent bulk flow), together with the calculated difference, and Figure 5b shows the same plot for comparison of I2 and the scaled measurements of JV. Figure 5a shows a clear large systolic peak in the difference graph indicating poor conformance between the predicted and measured venous flows whereas Figure 5B shows relatively good conformance.

Figure 6 also compares the pulsatility profiles of the predicted venous outflow I2 and the scaled measures of supratentorial flow (Ven). The curves are significantly different ($p < 0.05$, Wald-Wolfowitz test) with inter-group differences ($p < 0.05$, Mann Whitney test) at 5 of the 16 time points. Figure 7 shows the equivalent comparison between I2 and the scaled measurement of JV. There is a smaller delay between the peak of I2 and JV of approximately 6% of a cardiac cycle. A significant difference ($p < 0.05$, Mann Whitney test) between the individual measurements is seen at only one time point.

Table 2 shows the calculated values of the 7 relative variables derived from the model. A measurement of pressure at some point within the cerebral vasculature would be required in order to set the scaling of the model and provide absolute values of the parameters. However, a pressure measurement could not be obtained non-invasively; therefore, the parameters are given as relative values, normalised to R1. As expected the impedance values of

Parameter	Physical interpretation	Value	Standard error
R1	Impedance of arterial capillaries	1.0	0.0025
R2	Impedance of cerebral aqueduct	≈ 0.0	–
R3	Impedance of venous capillaries	≈ 0.0	–
R5	Impedance of arteries	0.01	8×1.8^{-3}
C1	Elastic capacitance of arteries	$\approx large$	–
C2	Elastic capacitance of ventricles	4.11	0.11
C3	Elastic capacitance of capillaries	≈ 0.0	5×10^{-3}
C4	Elastic capacitance of veins	271.017	18

Table 2: The estimated relative values for parameters R1-R5 and C1-C4 (see Fig. 2) together with their approximate physiological characteristics.

the aqueduct, venous capillaries and major arteries are very low whilst the arterial capillaries (including the pial resistance arterioles) is high. Elastic capacitance in the cerebral arteries is extremely high and cannot be accurately estimated from the model since it tends to infinity, whilst the elastic capacitance of the ventricles and of the cerebral capillary bed is very low (consistent with 0). The capacitance of the draining veins is intermediate in value, approximately 50 times higher than the ventricles but far lower than the major arteries.

4 Discussion

In normal, healthy individuals systolic expansion of the basal cerebral arteries produces a pressure wave within the subarachnoid CSF, which causes an outflow of CSF through the foramen magnum into the compliant spinal CSF space, equivalent to approximately 50% of the increase in intracerebral blood volume [11, 4]. The pressure wave is also transmitted to the major dural venous sinuses by systolic expansion of the arachnoid granulations [12, 20]. The effect of this is that the systolic pressure wave is dissipated into the formation of CSF and venous pulsatility and largely bypasses the cerebral circulation. In addition, elastic artery walls absorb part of the energy of the systolic pulse wave, which is then released during diastole, further flattening the arteriolar pressure profile to which the intracerebral circulation is exposed: this is known as the Windkessel effect. Constancy of cerebral perfusion pressure is also maintained by transient systolic increases in venous backpressure within the brain due to direct compression of cortical surface veins by the systolic pulse wave in the subarachnoid CSF space. This combination of processes maintains a constant perfusion pressure and flow in the cerebral capillary bed despite the major pressure changes seen between systole and diastole. Abnormalities of the mechanism have been described in a number of disease states including communicating hydrocephalus [11], normal pressure hydrocephalus (NPH) [3, 6], idiopathic intracranial hypertension (IIH) [5, 17], secondary intracranial hypertension (SIH) [5], ischaemic white matter change (leukoariaosis; LA) [4], neurodegenerative and mixed dementias, cerebral atrophy and vascular depression [7, 19] (i.e. geriatric depression associated with cerebrovascular disease). In some of these disease states it is now believed that abnormalities of this homeostatic mechanism form the major mechanism of injury, whereas in others it is unclear whether abnormalities simply reflect secondary effects.

One of the main problems associated with MR flow studies of Monro-Kelly homeostasis is the diversity of methodology used to analyse the data; there are few examples of coherent analysis approaches even in consecutive studies from single research groups. This variance largely reflects continuing confusion concerning the actual mechanism and its modes of failure and the need to tailor analyses to specific disease states. Previous workers have described theoretical electrical equivalence models of intracranial hydrodynamics and have tested them with simulated data sets [22, 23]. However, our previous study and the work presented here represent the first attempt to validate such a model with real data.

We have previously shown that the model describes the statistical variations observed in arterial and CSF waveforms in normal individuals [16]. In this study we have demonstrated that the model is capable of predicting the venous outflow waveform in the jugular vein with an acceptable level of accuracy, confirming the assumptions implicit in the simplified anatomical model (Figure 1) on which it is based. Nonetheless, a review of the literature indicates that it is likely to be over-simplistic for use in pathological conditions. Firstly, there is a clear functional dichotomy between the superficial and deep cerebral venous drainage territories, which are not represented separately in the model, in the way that they respond in different disease states [3, 6]. Secondly, there is a need to understand the distribution of systolic pulse wave energy within the superficial venous system and major dural venous sinuses, and thirdly, the variations in CSF flow in the supra and infra-tentorial compartments may require explicit modelling. In this study we showed that the major dural venous sinuses in the supratentorial compartment have a later and

less pronounced systolic waveform than those predicted by the model and observed in the jugular venous outflow. This supports the observations of previous workers that the infratentorial CSF dynamics are characterised by an early outflow of CSF from the fourth ventricle [2].

Recently, Alperin et al. have identified a temporal discrepancy between the fluid inflow (arterial) and outflow (venous plus CSF), which indicates the existence of small temporal fluctuations in intracranial volume [1]. They attribute these changes to inherent elastance in the brain substance and use the known relationships between pressure and flow to derive non-invasive estimates of intracranial pressure. We have also observed this discrepancy, which can be expressed as the difference between the scaled measurements of jugular venous outflow and the estimate (I2) provided by the model (Figure 5b). The shape and timing of this waveform are identical to that described by Alperin and colleagues [1] (Figure 5) although the measured peak-to-peak values in this study are slightly larger than the values they described in 8 volunteers (3.8 mls/heartbeat beat to beat versus 0.3-1.3 mls/heartbeat). One potential shortcoming of the current study was the decision to measure flow patterns in the hindbrain circulation from the mid-portion of the basilar artery. This was done in order to ensure that the measured waveform was truly characteristic of the intracranial arterial tree, which may differ from that seen in the vertebral arteries. It was expected to lead to a systematic underestimation of the arterial blood flow volume, which was indeed evident in the comparisons of prosencephalic arterial and venous flow volume, where CAB was almost equivalent to Ven in some individuals. It may also underlie the minor differences in intracranial volume change described above. In practice this can easily be corrected by using the volume measurements from the vertebral arteries to scale the waveform from the basilar artery for use in the model.

Although the current study represents a validation of a simplified model in normal subjects it is clearly appropriate for the study of diseases where the principle abnormalities lie in the arterial inflow waveform (such as hypertension, elevated pulse pressure), the arterial tree (such as arterial stenosis, vascular depression, vascular dementia, IICH), or the compliance of the brain itself. The application of the model to these and similar disorders is likely to improve our understanding of the pathological mechanisms involved through its ability to support statistical inter-group comparisons of physiological variables that are currently not measurable (arterial compliance, brain compliance, ventricular compliance, overall venous compliance, arterial impedance, brain impedance and the impedance of the cerebral aqueduct). However, although the model could be applied to the characterisation and study of other disorders, such as veno-occlusive diseases, it is unlikely to provide the desirable level of granularity to explore the underlying anatomical and physiological mechanisms involved. There is therefore a need for further extension of the model to support such studies. Explicit modelling of the contributions of the supratentorial and infratentorial compartments is likely to be relatively straightforward as variations in the waveforms of the major supratentorial dural venous sinuses are directly measurable. The addition of a measurement of CSF flux through the incisura is straightforward, although the fourth ventricular outflow may have multiple outflow pathways. More importantly, it is possible to measure pulsatile venous flow at other sites in the venous system including the straight sinus, sigmoid and transverse sinuses, extracerebral jugular vein and major superficial cortical veins such as the Great Vein of Labbe, which represent the principal collateral venous flow mechanism from the prosencephalic cortex. The use of these measurements may support extension of the model to allow differentiation of the pressure effects on deep cerebral, superficial cortical and dural veins, which have been proposed as aetiological factors in various disorders [3, 4, 5, 6, 7].

5 Conclusion

We have described a simplified anatomical model of Monro-Kellie homeostasis, and presented an electrical equivalence model that allows derivation of values corresponding approximately to arterial, brain, ventricular and venous compliance, and arterial, brain, and cerebral aqueduct impedance. We have validated the model by showing its ability to predict jugular venous waveform in normal subjects and have identified a number of potential applications where the use of the model can be expected to improve our ability to understand the mode of failure of the homeostatic mechanism.

6 Acknowledgements

Authors would like to thank Dr. Marietta Scott for her helpful comments and Mr. Barry Whitnall for his role in scanning and collecting MR data.

Appendix 1

This section describes the derivation of a minimal descriptive model for the circuit shown in Figure 2b and the fitting approach used to estimate individual parameters. The application of Kirchoff's laws leads to

Vertex Currents:

$$I_1 = I_5 + I_6 \tag{1}$$

$$I_8 = I_9 + I_2 \tag{2}$$

$$I_6 = I_3 + I_7 + I_8 \tag{3}$$

$$I_4 = I_5 + I_3 + I_7 + I_9 \tag{4}$$

Voltage loops:

$$I_5 R_5 = I_5 \frac{1}{j\omega C_1} - I_3 R_2 - I_3 \frac{1}{j\omega C_2} - I_6 R_1 = 0 \tag{5}$$

$$I_7 \frac{1}{j\omega C_3} - I_9 \frac{1}{j\omega C_4} - I_8 R_3 = 0 \tag{6}$$

$$I_3 \frac{1}{j\omega C_2} + I_3 R_2 - I_7 \frac{1}{j\omega C_3} = 0 \tag{7}$$

Point-to-point voltages:

$$V_2 - V_1 = I_6 R_1 + I_8 R_3 + I_2 R_4 \tag{8}$$

$$V_3 - V_1 = I_6 R_1 + I_3 \frac{1}{j\omega C_2} + I_3 R_2 + I_4 \frac{1}{j\omega C_5} \tag{9}$$

In these equations I is frequency and j is $\sqrt{-1}$. We have introduced 5 new current variables (I5 to I9), and we have 9 equations, leaving 6 degrees of freedom. The point-to-point voltages require the equivalent of pressure measurements in the biological system. After eliminating unwanted variables, and using the notational convention $D_{n\omega} = 1/j\omega C_n$, we have obtained three important equations to note: the Monro-Kellie Principle Eq. 10, which is simply a statement of volume preservation; the constraint equation Eq. 11 relating currents, which does not contain I_1, C_5 or R_4; and Eq. 12, which scales the variables using mean potentials.

Monro-Kellie Principle:

$$I_1 = I_2 + I_4 \tag{10}$$

Constraint equation relating currents (flows):

$$\begin{aligned}(R_5 + D_{1\omega} + R_1)[I_3(D_{2\omega} + R_2)(D_{3\omega} + D_{4\omega} + R_3) - D_{3\omega}(I_4 - I_3)D_{4\omega} - D_{3\omega}(I_4 - I_3 + I_2)R_3] \\ + D_{3\omega}[I_3(R_2 + D_{2\omega}) + (I_2 + I_4)R_1](R_3 + D_{4\omega}) = 0\end{aligned} \tag{11}$$

Using mean potentials (pressures) to scale variables:

$$< V_3 > - < V_1 > = < I_1 > R_1 \tag{12}$$

Parameter Estimation

A likelihood-based approach was adopted in order to estimate the parameters of the model. We can build a suitable likelihood function from Eq. 11. Substituting Eq. 10 and re-organising terms, we obtain an equation of the form

$$\gamma I_3 - \alpha I_1 + \beta I_4 = 0 \tag{13}$$

We can now make corrections to the flow variables ΔI_n in order to enforce the constraint equations, in a way that minimises the change in the measurements consistent with the measurement errors σ_n,

$$\chi^2 = \sum_{\omega} \Delta I_1^* \Delta I_1 / \sigma_1^2 + \Delta I_3^* \Delta I_3 / \sigma_3^2 + \Delta I_4^* \Delta I_4 / \sigma_4^2 \tag{14}$$

References

[1] N J Alperin, S H Lee, and F Loth. MR-intracranial pressure (ICP): a method to measure intracranial elastance and pressure noninvasively by means of mr imaging: baboon and human study. *Radiology*, 217(3):877–85, 2000.

[2] O Baledent, M C Henry-Feugeas, and I Idy-Peretti. Cerebrospinal fluid dynamics and relation with blood flow: a magnetic resonance study with semiautomated cerebrospinal fluid segmentation. *Invest Radiol*, 36(7):368–77, 2001.

[3] G A Bateman. Vascular compliance in normal pressure hydrocephalus. *AJNR Am J Neuroradiol*, 21(9):1574–85, 2000.

[4] G A Bateman. Pulse-wave encephalopathy: a comparative study of the hydrodynamics of leukoaraiosis and normal-pressure hydrocephalus. *Neuroradiology*, 44(9):740–8, 2002.

[5] G A Bateman. Vascular hydraulics associated with idiopathic and secondary intracranial hypertension. *AJNR Am J Neuroradiol*, 23(7):1180–6, 2002.

[6] G A Bateman. The reversibility of reduced cortical vein compliance in normal-pressure hydrocephalus following shunt insertion. *Neuroradiology*, 45(2):65–70, 2003.

[7] G A Bateman. Pulse wave encephalopathy: a spectrum hypothesis incorporating Alzheimer's disease, vascular dementia and normal pressure hydrocephalus. *Med Hypotheses*, 62(2):182–7, 2004.

[8] S C Beards, S Yule, and A Kassner. Anatomical variation of cerebral venous drainage: the theoretical effect on jugular bulb blood samples. *Anaesthesia*, 53(7):627–33, 1998.

[9] D A Bennett and M P McDermott. Cerebrospinal fluid shunting for Alzheimer's disease? *Neurology*, 59(8):1126–7, 2002.

[10] H Cushing. *The third circulation in studies in intracranial physiology and surgery*. Oxford University Press, London, 1926.

[11] D Greitz. Radiological assessment of hydrocephalus: new theories and implications for therapy. *Neurosurg Rev*, 27(3):145–65, 2004.

[12] D Greitz, T Greitz, and T Hindmarsh. A new view on the CSF-circulation with the potential for pharmacological treatment of childhood hydrocephalus. *Acta Paediatr*, 86(2):125–32, 1997.

[13] D Greitz, J Hannerz, and T Rahn. MR imaging of cerebrospinal fluid dynamics in health and disease. on the vascular pathogenesis of communicating hydrocephalus and benign intracranial hypertension. *Acta Radiol*, 35(3):204–11, 1994.

[14] V B Joseph, L Raghuram, and I P Korah. MR ventriculography for the study of CSF flow. *AJNR Am J Neuroradiol*, 24(3):373–81, 2003.

[15] J Kim, P A Bromiley, and N A Thacker. A complexity analysis for normal cerebral blood and CSF flow. In *Proc MIUA 05, Bristol, 19-20 July 2005*, pages 67–70, 2005.

[16] J Kim, N A Thacker, P A Bromiley, and P C W Beatty. An electrical equivalence model for CSF pulsatility. In *Proc. 17th Biennial International EURASIP Conference (BIOSIGNAL), Brno, Czech Republic, 23-25 June 2004*, pages 431–433, 2004.

[17] N T Mathew, J S Meyer, and E O Ott. Increased cerebral blood volume in benign intracranial hypertension. *Neurology*, 25(7):646–9, 1975.

[18] T Miyati, M Mase, and T Banno. Frequency analyses of CSF flow on cine MRI in normal pressure hydrocephalus. *Eur Radiol*, 13(5):1019–24, 2003.

[19] J Naish. Abnormalities of CSF flow patterns in the cerebral aqueduct in treatment resistant late life depression: a potential biomarker of microvascular angiopathy. *MRM. Mag Reson Med*, page In Press, 2007.

[20] E Stolz, M Kaps, and A Kern. Transcranial color-coded duplex sonography of intracranial veins and sinuses in adults. reference data from 130 volunteers. *Stroke*, 30(5):1070–5, 1999.

[21] C Strik, U Klose, and M Erb. Intracranial oscillations of cerebrospinal fluid and blood flows: analysis with magnetic resonance imaging. *J Magn Reson Imaging*, 15(3):251–8, 2002.

[22] M Ursino and C A Lodi. A simple mathematical model of the interaction between intracranial pressure and cerebral hemodynamics. *J Appl Physiol*, 82(4):1256–69, 1997.

[23] M Ursino and C A Lodi. Interaction among autoregulation, CO2 reactivity, and intracranial pressure: a mathematical model. *Am J Physiol*, 274(5(2)):H1715–28, 1998.